Nanoscale Investigations of α- and γ-Crystal Phases in PVDF-Based Nanocomposites

Sophie Barrau, Anthony Ferri, Antonio Da Costa, Juliette Defebvin, Sébastien Leroy, Rachel Desfeux, Jean Marc Lefebvre

Nanoscale investigations of α- and γ-crystal phases in PVDF based nanocomposites

Sophie Barrau,[1] *Anthony Ferri,*[2] *Antonio Da Costa,*[2] *Juliette Defebvin,*[1] *Sébastien Leroy,*[2] *Rachel Desfeux*[2] *and Jean-Marc Lefebvre*[1]

[1] Université Lille, Sciences et Technologies, CNRS, Unité Matériaux Et Transformations (UMET), F-59000 Lille, France

[2] Université Artois, CNRS, Centrale Lille, ENSCL, Université Lille, UMR 8181, Unité de Catalyse et Chimie du Solide (UCCS), F-62300 Lens, France

KEYWORDS

PVDF, γ-phase, atomic force microscopy, carbon nanotubes, piezoelectric

ABSTRACT

The impact of carbon nanotubes (CNTs) incorporation into semi-crystalline poly(vinylidene fluoride), PVDF, was investigated at both macro- and nanoscales. A special effort was devoted to probe the local morphology, and mechanical, ferroelectric, piezoelectric and electrical conductivity response by means of atomic force microscopy tools. Incorporation of CNTs mainly induces the development of the polar γ-phase and as a consequence the coexistence of the γ-phase with the most stable non-polar α-phase is observed. A maximum γ-phase content is reached at 0.7 wt% CNT loading. The spherulitic morphology of the PVDF α-phase is assessed, in conjunction with the lack of any ferroelectric response, while the presence of the polar γ-phase is confirmed, owing to clear piezoresponse signals. Local piezoelectric measurements on γ-phase domains yield a maximum effective coefficient $|d_{33}|$ ~13 pm/V, thus underlining the potential for applications of such functional PVDF-based nanocomposites in advanced piezoelectric devices. An increase in macroscopic conductivity with CNT content is observed, with a percolation threshold achieved for a composition close to 0.7 wt%. Nanoscale investigation of electrical conductivity confirms the presence of some infinite CNT cluster homogeneously distributed over the surface. The macroscopic viscoelastic behavior of the composite reflects the reinforcing effect of CNTs, while the nanomechanical characterization yields a local contact modulus of the γ-phase domains larger than that of its α-phase counterpart, in agreement with the fact that the CNTs act as γ-phase promoters and subsequently reinforce the γ-domains.

INTRODUCTION

Polymers with electroactive properties provide numerous opportunities for applications in domains such as biomedicine or energy generation owing to their flexibility, good mechanical acoustic impedance and biocompatibility compared to ceramic materials. Among this class of polymers, poly(vinylidene fluoride) (PVDF) is a semi-crystalline polymer with unique piezo-, pyro- and ferroelectric properties allowing its use for various development in sensors, actuators and energy harvester systems.[1] PVDF displays a complex crystal polymorphism with three main phases of interest α, β and γ.[2] The non-polar α-phase (TGTG' conformation) is the most common phase, obtained directly by cooling from the melt at conventional rates.[3] The electroactive properties are mainly related to the highly polar β-phase (TTTT conformation) induced by stretching films initially in α-phase or in the presence of fillers.[4] The intermediate polar γ-phase (TTTGTTTG' conformation)[5] focuses attention as a ferroelectric material and because it provides a higher breakdown strength and discharge energy density as compared to the β-phase.[6] This phase may either be obtained by isothermal crystallization at high temperature,[7] or by solution induced crystallization[8] or as well by filler addition. Indeed fillers such as clays,[9,10] zeolites[11] or carbon based fillers[12,13] may promote the formation of the γ-phase owing to the existence of favorable interactions between the polymer chains and the filler surface. For instance a 0.2 wt% content of montmorillonite (MMT) clay induces a γ-phase content of 36%.[14] Filler addition may also impact material properties. For instance, carbon nanotubes (CNTs) can improved the dielectric and piezoelectric behavior of fluorinated polymer.[15] However, there still remains a key scientific issue in the understanding of how the behavior of pristine PVDF or PVDF composites at the nanoscale impacts the macroscopic properties. Some studies at local scale have already been reported in the literature on thin films[16-19] or fibers[20-22] but have been primarily focused on the β-phase. To our knowledge, no

deep investigation at the nanoscale on both microstructure and physical properties of the γ-phase, has been reported in the literature.

In the present study, the γ-phase was induced by dispersion of CNTs in the polymer matrix. The morphology of the co-existing crystal polymorphs was investigated and correlated to the nanoscale ferroelectric, piezoelectric, electrical conductivity and mechanical response by means of advanced tools of atomic force microscopy (AFM). Identification of the two major PVDF crystal phases (namely α and γ-phases) in the nanocomposites was achieved and the impact of the CNTs on the physical properties was probed at local scale.

EXPERIMENTAL SECTION

Materials. PVDF (Kynar® grade 720) was provided by Arkema. Multiwalled CNTs (8.5 nm in diameter and 1.5 μm in length) were obtained from Nanocyl (Nanocyl 7000 series, Belgium).

Elaboration of CNT-PVDF nanocomposites. Nanocomposites were elaborated following a two-step procedure. CNTs and PVDF were dispersed in N,N-dimethylacetamide (DMAc) (Sigma-Aldrich). The solution was stirred at 40°C for 1h and was subsequently poured into silicone cups and left overnight at ambient temperature and atmospheric pressure (T_{amb}, P_{atm}). The residual solvent was removed by placing the nanocomposites in a vacuum oven at 40°C for 10h. Then the "dried" material was melt-compounded using a twin-screw microextruder from DSM Xplore (Geleen, The Netherlands) under the following conditions (210°C, 50 rpm, 5 min under nitrogen atmosphere). The extrudates with a 2 mm diameter were air-cooled at the exit of the die. The samples are denoted NTx where x holds for the CNT content in wt%, namely NT0 for neat PVDF, NT01, NT03, NT07, NT1 and NT12 for composites with 0.1, 0.3, 0.7, 1.0 and 1.2 wt% loading, respectively.

Nanocomposite thin film preparation. Thin films were prepared by spin coating on silicon wafers coated with platinum. The nanocomposite previously elaborated was solubilized in

DMAc and the solution was deposited at ambient temperature with a rotational speed of 2000 rpm for 20 s and at an acceleration of 200 $m.s^{-2}$.

Characterization. Fourier transform infrared (FTIR) spectra were collected after 16 scans (resolution of 2 cm^{-1}) using-ATR (Attenuated Total Reflexion) technique on a Perkin Elmer Spectrum 100 spectrometer. Wide-angle X-ray scattering (WAXS) measurements were performed from a Cu target (λ = 1.54 Å), operated at 20 mA and 40 kV. The sample-to-detector distance was 6 cm. 2D-WAXS patterns were recorded on a CCD camera from Photonic Science Ltd and the radial WAXS intensity profiles were obtained by azimuthal integration using the FIT2D software. Thermal characterization was performed on a DSC Q20 (TA Instruments) calibrated with indium under nitrogen atmosphere. Samples of approximately 10 mg were put in aluminum pans and were analyzed between 20 and 200°C at a heating rate of 20°C.min^{-1} under nitrogen gas flow. The morphology of nanocomposites was investigated by field emission scanning electron microscopy (FE-SEM) using an Hitachi S4700 apparatus operated at an acceleration voltage of 10 kV. The micrographs were taken from the surface of cryofractured samples previously coated with carbon. Nanoscale measurements were performed by AFM using a commercial microscope (Asylum Research/Oxford Instruments, MFP-3D, USA) working in air at room temperature. Electroactive properties were probed by recording piezoelectric hysteresis loops using dual AC resonance tracking (DART) piezoresponse force microscopy (PFM).[23] Such experiments were carried out using grounded conductive bottom electrode while Pt/Ir-coated silicon tips and cantilevers with a stiffness of 2.5 $N.m^{-1}$ (Nanosensors) were used.[24] Typical contact-resonance curves obtained during PFM experiments are presented in Figure S1. On macroscale, conductivity measurements were conducted at a frequency of 10-1 Hz by Broadband Dielectric Spectroscopy (Novocontrol BDS 4000 system). Local conductivity (*i.e.* current detection) was detected by the ORCA conductive-AFM technique. Similar tips as for PFM experiments were used. A bias voltage of

0.5 V was applied between the grounded tip and the conductive bottom electrode during mapping. For the nanoscale I-V spectroscopy, the DC bias was ranging between –10 and +10 V. Dynamic Mechanical Analysis (DMA) was performed on an Ares apparatus from TA Instruments used in torsion mode. Experiments were performed at a frequency of 1 Hz, in the temperature range –30°C < T < 30°C at a heating rate of 5 °C.min^{-1}. Nanomechanical response was probed by the AM-FM (amplitude modulation – frequency modulation) method from Asylum Research/Oxford Instruments,[25-27] using blueDriveTM photothermal excitation on a Cypher S AFM at 2 Hz (further details in Figure S2a). AC160TSA silicon tips (Olympus) with cantilever stiffness of 26 N.m^{-1} were used for these experiments and the tip/sample interaction was measured in the repulsive regime, which enables to get the contact modulus of the different PVDF phases. A reference polycarbonate sample with known modulus of 2.5 GPa was used to accurately adjust the model parameters such as the tip radius.[25]

RESULTS AND DISCUSSION

Characterization of the polymer crystal structure in nanocomposites combined FTIR, DSC and WAXS. Results are presented in Figure 1a-c.

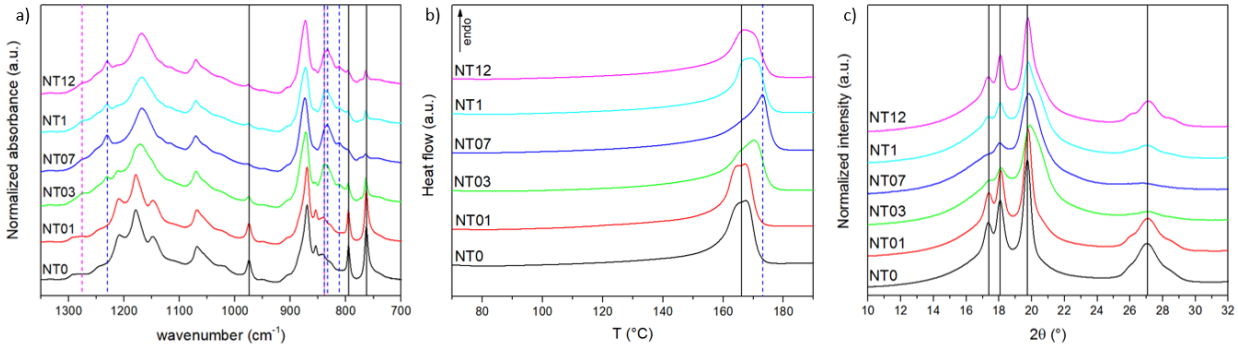

Figure 1. Structural characterization of the CNT-PVDF composites. (a) FTIR spectra, (b) DSC thermograms and (c) WAXS intensity profiles of nanocomposites. Vertical markers: black solid lines refer to PVDF α-phase, blue dash lines to PVDF γ-phase and magenta dash line to PVDF β-phase.

The NT0 FTIR spectrum exhibits the characteristic bands at 766 cm^{-1} (CF_2 bending and skeletal bending), 795 cm^{-1} (CH_2 rocking) and 976 cm^{-1} (CH out-of-plane deformation) associated to the presence of the PVDF α-phase. After CNT incorporation, the FTIR spectra of composites present additional bands at 812 cm^{-1} (CH_2 out-of-plane wag), 833 cm^{-1}, and 1234 cm^{-1} (CF out-of-plane deformation) as a signature of the PVDF γ-phase and a band at 1275 cm^{-1} corresponding to the PVDF β-phase.[28] Note the band at 840 cm^{-1} (CH_2 rocking) is attributed to both γ- and β-phases. FTIR data thus assess the coexistence of the three α-, γ- and β-phases in the nanocomposites. It appears that β- and γ-phase development is not linearly dependent on CNT content. Indeed, for both polar crystal phases, band intensities increase with CNT content up to a maximum value reached for NT07 and then decrease at higher CNT content. Assessment of the degree of crystallinity and of the respective fractions of the different crystal polymorphs has been performed through the combined analysis of FTIR and DSC data. According to the method recently developed by Cai et al.[28] for FTIR data treatment in the particular case of the co-existence of the three crystal phases, the relative fraction of the electroactive γ- and β-phases (F_{EA}) was first calculated. Then quantification of individual γ- and β-phase contributions has been performed by focusing on their specific signatures at 1234 cm^{-1} and 1275 cm^{-1} respectively. The relative fractions (F) of electroactive (EA), α-, γ- and β-phases in the composites are reported in Table 1. The key information issued from the FTIR analysis is that the β-phase is a minor component of the polar fraction. Complementary information to estimate the degree of crystallinity and the crystal phase fraction of α- and γ-phases is provided by DSC measurements The DSC thermograms display the melting peak of PVDF α-phase at 165°C. A shoulder at 173°C, characteristic of the γ-phase,[29] is also present beyond 0.3 wt% CNT content, and it is more pronounced for NT07. The β-phase fraction is considered negligible and the

enthalpy of fusion for a 100% γ-phase PVDF is assumed identical to that of a 100% α-phase ($\Delta H_{\alpha,100}$ = 93.07 J/g).[8] The results are also reported in Table 1. At first sight WAXS diffractograms are definitely not providing sound information with respect to the relative composition in crystal phases. Indeed, the characteristic peaks of PVDF α-phase are observed at 2θ = 17.4°, 18.1°, 19.7° and 26.7°, corresponding to the (100), (020), (110) and (021) planes respectively.[30,31] Regarding the β-phase, the main diffraction peak attributed to the (110/200) planes is located at 2θ =20.6° and superimposed to those of the α-phase. In the case of the γ-phase the characteristic peaks at 2θ = 19.2° and 20.04° corresponding to the (020) and (110/101) planes are as well superimposed to those of the α-phase in the 20° region. A broadening of the latter peak in this particular angular range may however be noticed for NT07 in relation to the coexistence of the α and γ phases. The diffraction peak at 2θ = 26.7° related to the α-phase nevertheless provides an indirect way to probe the evolution of γ-phase content. The intensity of the diffraction peak decreases at low CNT content, reaches a minimum for NT07 and then increases again at higher CNT content, thus suggesting that the γ-phase content is indeed maximum for NT07 as probed by FTIR and DSC.

Table 1. Degree of crystallinity χ and relative fraction (F) of electroactive (EA), α-, γ- and β-phases of PVDF.

	χ (%) [a]	F_{EA} (%) [b]	F_α (%) [a, b]	F_γ (%) [a, b]	F_β (%) [b]
NT0	60.7	0	100, 100	0, 0	0
NT01	59.3	0.2	100, 99.8	0, 0	0.2
NT03	58.0	33.9	60.9, 66.1	39.1, 33.2	0.7
NT07	55.4	46.7	58.6, 53.3	41.4, 45.7	1
NT1	57.1	39.5	59.9, 60.5	40.1, 38.7	0.8
NT12	57.7	37.8	60.3, 62.2	39.7, 37.0	0.8

[a] determined by DSC

[b] by FTIR according to the procedure developed in ref[28]

A fair agreement is obtained between FTIR and DSC analysis. Incorporation of carbon nanotubes not only induces a change in PVDF crystal phase but seems to impact as well the overall degree of crystallinity in the nanocomposites. There remains however reasonable doubt about the assumption of identical enthalpy of fusion for both α- and γ-phases. In the following, contribution of the β-phase fraction will be considered negligible in the nanoscale investigation of properties.

To sum up, the structural characterization of nanocomposites reveals that incorporation of carbon nanotubes mainly induces the development of the polar PVDF γ-phase, and a maximum γ-phase fraction is observed at 0.7 wt% CNT content. Recently Kumar *et al.*[32] established that the γ-phase fraction is dependent on CNT functionalization and composite processing, and in all cases, increases with CNT. As stated above, this is not the case in the present study. Considering that a maximum γ-phase content is reached for NT07 and then decreases at higher CNT content, there ought to be a limitation to γ-phase formation beyond this particular composition.

Assessment of the state of dispersion of the CNTs in the polymer matrix is essential to understand the nanocomposite behavior. Figure 2a shows the SEM micrograph of NT07 as probed on the cryofractured surface of a bulk specimen.

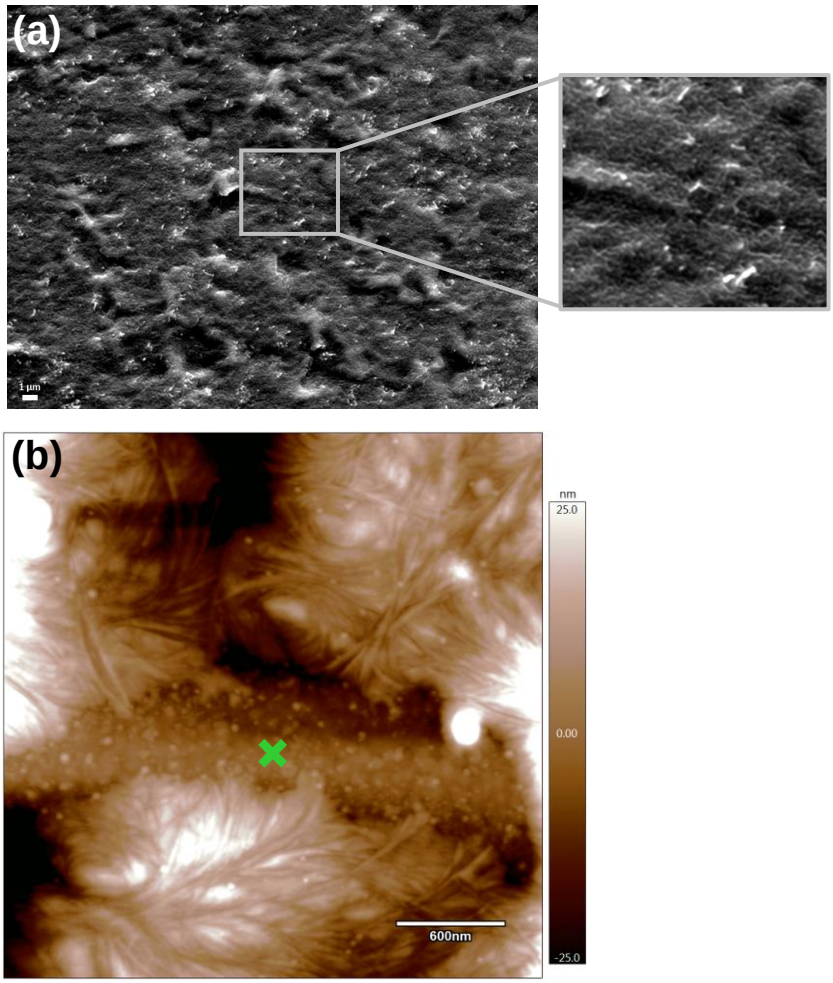

Figure 2. Surface morphology of the NT07 composite film. (a) SEM image of cryofractured surface of NT07 composite presenting the CNT distribution, and (b) AFM topographic image of NT07 thin film composite showing PVDF α-phase spherulites. The green cross refers to the postulated γ-phase zone.

CNT distribution in the polymer matrix appears fairly homogeneous at the micrometer scale, as evidenced by the white contrasts. However, at a lower scale, isolated CNTs as well as CNT aggregates may be observed. The thin film surface morphology of NT07 was recorded by AFM over a 3×3 µm² scan as illustrated in Figure 2b. Lamellae organized into spherulites as classically seen in semi-crystalline polymers are clearly observed with high spatial resolution. The thickness of individual lamellae is around 10 nm. This morphology is characteristic of the

PVDF α-phase. In the meantime, some areas display an irregular shape (as indicated by the green cross on Figure 2b) with a topographic contrast similar to those of α-spherulites. At this stage, we may postulate that it might refer to the presence of γ-spherulites located between α-phase spherulites, thus avoiding α-spherulite impingement. The γ-spherulites are known to exhibit a rather odd bundle type arrangement of crystalline lamellae with "scroll-like" morphology.[33,34] These nanoscale morphological features are not evidenced on the present figure.

To better distinguish the two PVDF phases, the local electroactive behavior was probed at various locations over the entire surface of the thin film by using the spectroscopic tool of the PFM. The probing tip was used as nanometric top electrode over the surface to locally assess the polarization switching and the electromechanical activity. The piezoresponse loops were achieved in remnant mode, *i.e.* at zero voltage, to avoid electrostatic interactions.[35] To illustrate this investigation, an example of scanned surface recorded on larger area (10×10 μm²) than for the previous AFM image (Figure 2b) is depicted on Figure 3a, where the two characteristic morphologies described above are seen. Several locations symbolized by the numbered crosses were analyzed on this scan area, which reflect the electrical response of the whole sample. Both phase and amplitude PFM signals obtained are shown on Figure 3b and 3c, respectively.

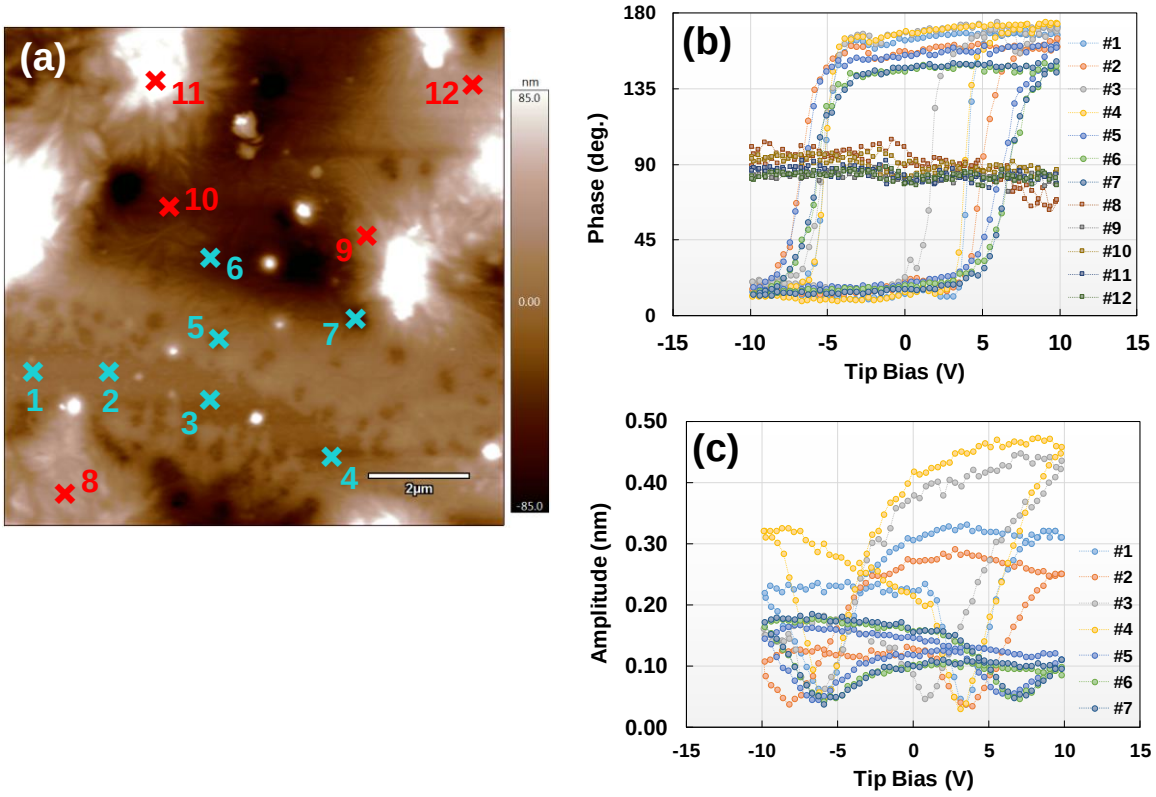

Figure 3. Local electroactive behavior of the NT07 composite. (a) AFM surface morphology, (b) remnant phase and (c) remnant amplitude PFM loops recorded at the marked location on the nanocomposite surface. For clarity, the absence of signal observed at the locations numbered 8 to 12 are plotted on the phase PFM graph in (b) only.

As expected, no ferroelectric signal is measured in the spherulitic zones attributed to the non-polar PVDF α-phase and identified as red crosses on the AFM image (see Figure 3b). On the contrary, in the areas indicated by the blue crosses numbered from 1 to 7, well-defined ferroelectric loops with two stable states of polarization for phase signal and typical butterfly-shape for amplitude response are obtained, as revealed on Figures 3b and 3c. This is directly related to the polar nature of the PVDF phase under investigation, *i.e.* to the ferroelectric γ-phase previously mentioned. As a remark, both coercive voltage and vibration amplitude deduced from the phase and amplitude loops respectively are not similar for the seven recorded signals. This can be explained by the complex nature of the probed volume under the tip, where

amorphous phase and CNTs as well as crystalline γ-phase coexist. By considering the piezo-activity at maximum applied voltage for the higher amplitude-voltage butterfly signal (loop #4), the larger local deformation of the film due to the converse piezoelectric effect is 450 pm. However, this latter value was overestimated owing to the DART PFM method used for the measurement in which the contact resonance of the cantilever enhances the detected PFM signal. Moreover, in the case of a polymer material, relatively high losses are considered resulting in a lower Q quality factor of the cantilever of about 10.[36-38] Thus, by considering the expression $A = d_{33}V_{ac}Q$,[36,37] where A is the detected PFM amplitude and V_{ac} the driving voltage (3.5 V for our measurements), we can estimate the maximum effective piezoelectric coefficient $|d_{33}|$ around 13 pm/V (note that the d_{33} piezoelectric coefficient of PVDF is negative). This value is lower than –58.5 pm/V reported by Kanik *et al.* by the similar PFM technique for γ-phase PVDF nanoribbons.[39] However, in the latter case the high effective piezoelectric constant was mainly attributed to the nanoscale confinement, where a larger contribution of the domain wall motion occurs. In the present study, the estimated value is more in agreement with –7 pC/N measured at the macroscopic scale on PVDF γ-phase based nanocomposites,[10] the difference could be explained by a nanoscale confinement as mentioned above but with a reduced effect. This is quite significant with respect to the polymeric nature of the electromechanical layer and the absence of polarization step before d_{33} measurement, opening perspectives for the integration of such nanocomposites in piezoelectric-based applications.

As a result, the presence of both α- and γ-phases is thus confirmed by probing the nanoscale morphology and the PFM ferroelectric and piezoelectric response. AFM data of mixed α- and γ-phases have already been published by Cebe *et al.*[40] in the case of PVDF nanocomposites incorporating organically modified clay silicates, however not at such nanometric resolution. Contrary to our observations, these authors report that the γ-spherulites lie on top of the α-spherulites. This morphology is explained by clay migration to the surface during the melt-

crystallization process, while clays act as a promoter of the PVDF γ-phase. The 2D nature of the clay platelet and its propensity to lie parallel to the surface is definitely the key factor that yields the difference with our present situation dealing with rod-like nano-reinforcement. Otherwise, considering that solvent evaporation at ambient temperature is very slow, any memory of the initial mechanical centrifugation of the spin-coating process should be erased prior to full evaporation. No resulting chain orientation is thus expected. For the sake of comparison, the AFM image of NT07 surface of a thick film is shown in Figure S3.

In order to understand the influence of CNTs on the structural evolution of PVDF (presence of a maximum in γ-phase content), electrical measurements have been performed. The evolution of electrical conductivity as a function of CNT content is reported in Figure 4a.

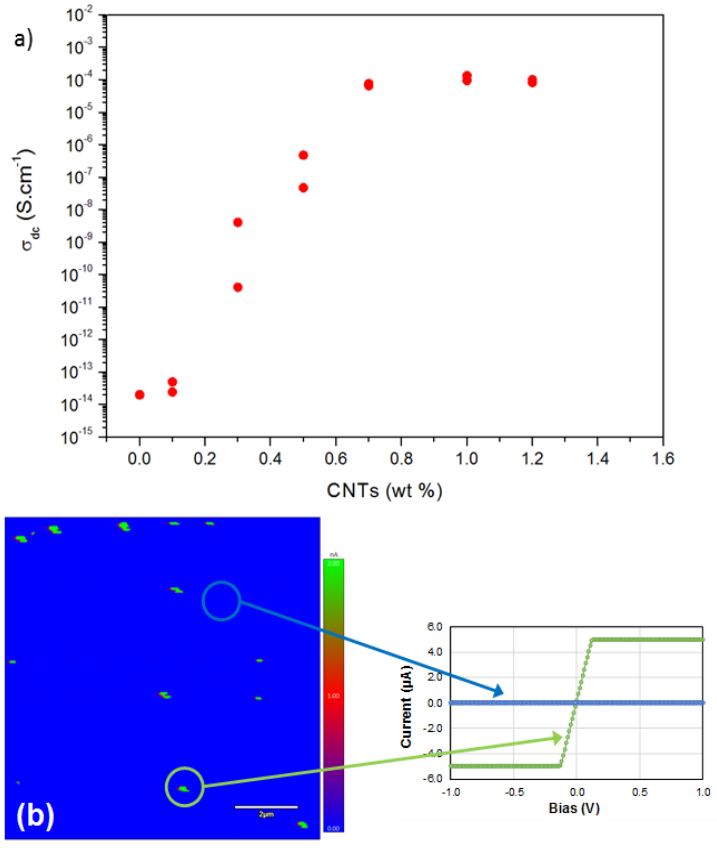

Figure 4. Electrical conductivity properties of the CNT-PVDF composite films. (a) Evolution of the DC conductivity as a function of CNT content and (b) local current mapping with associated I-V characteristics (5 µA is the detection limit of our system).

NT0 is an insulating material. Its electrical conductivity has a value of 2×10^{-14} S.cm^{-1}. The incorporation of a low amount of CNTs (NT01) implies the presence of finite size conductive clusters inside the polymer matrix that have no impact on electrical conductivity. Beyond 0.2 wt% CNT loading, the composites display a dramatic increase in σ_{dc} by 10 orders of magnitude to reach a value of 8×10^{-5} S.cm^{-1}. The percolation threshold, defined at 0.7 wt% of CNTs, indicates the existence of an infinite size conductive cluster within the PVDF matrix. The singularity in the PVDF crystal phase evolution with CNT content thus seems correlated to the electrical percolation threshold. A similar discontinuity of properties at the percolation threshold has already been reported in literature.[41,42] In the latter case, a glass transition temperature depression was observed. The free volume accessible to macromolecular motions and/or the specific interactions between the conducting fillers and the polymer matrix depending on the conductive network could explain the phenomenon. The existence of this singularity as a function of composition is further supported by the observation of a maximum in crystal growth as shown in Figure S4.

The specific mechanism is however still not fully understood. In the present situation it may be postulated that CNTs promote the formation of PVDF γ-phase. However CNT aggregation beyond NT07 composition reduces the capacity for CNT to further enhance surface nucleation.

The local conductivity was then probed over the surface of the NT07 sample by the ORCA c-AFM technique. Current map over 10×10 μm² is displayed on Figure 4b where conducting paths (green contrast) are observed, embedded in blue background contrast associated to the absence of signal. Such "hot spots" evidence the electrical conductivity of some areas in the sample, in agreement with the macroscopic measurements previously shown in Figure 4a. Local I-V characteristics were further performed on both insulating (blue) and conductive (green) regions (Figure 4b). As expected, Ohmic behavior is obtained when hot spots are locally probed

thus reflecting the occurrence of an electrical percolation path through the composite layer between the top (AFM tip) and bottom (platinum) electrodes, while no current signal is detected for the background region when the bias voltage is varied between –10 V and +10 V (figure plotted between –1 V and +1 V for clarity), confirming the insulating nature of the matrix. Therefore the conductive properties of NT07 observed at the macroscopic scale actually result from the presence of some infinite cluster (density of ~15 in the 10×10 μm^2 area) homogeneously distributed. Note that since NT07 is an electrically conductive sample, this precludes the measurement of macroscopic ferroelectric and piezoelectric properties, which further justifies the use of nanoscale probe to gain access to such electrical behavior.

Finally, the mechanical behavior of nanocomposites was analyzed by probing the dynamic viscoelastic response by DMA at a frequency f = 1 Hz. The storage modulus (G') of NT0 and NT07 recorded in the temperature range [–30°C, +30°C], *i.e.* above the glass transition temperature and below the melting temperature of secondary crystals,[43] is displayed in Figure 5a.

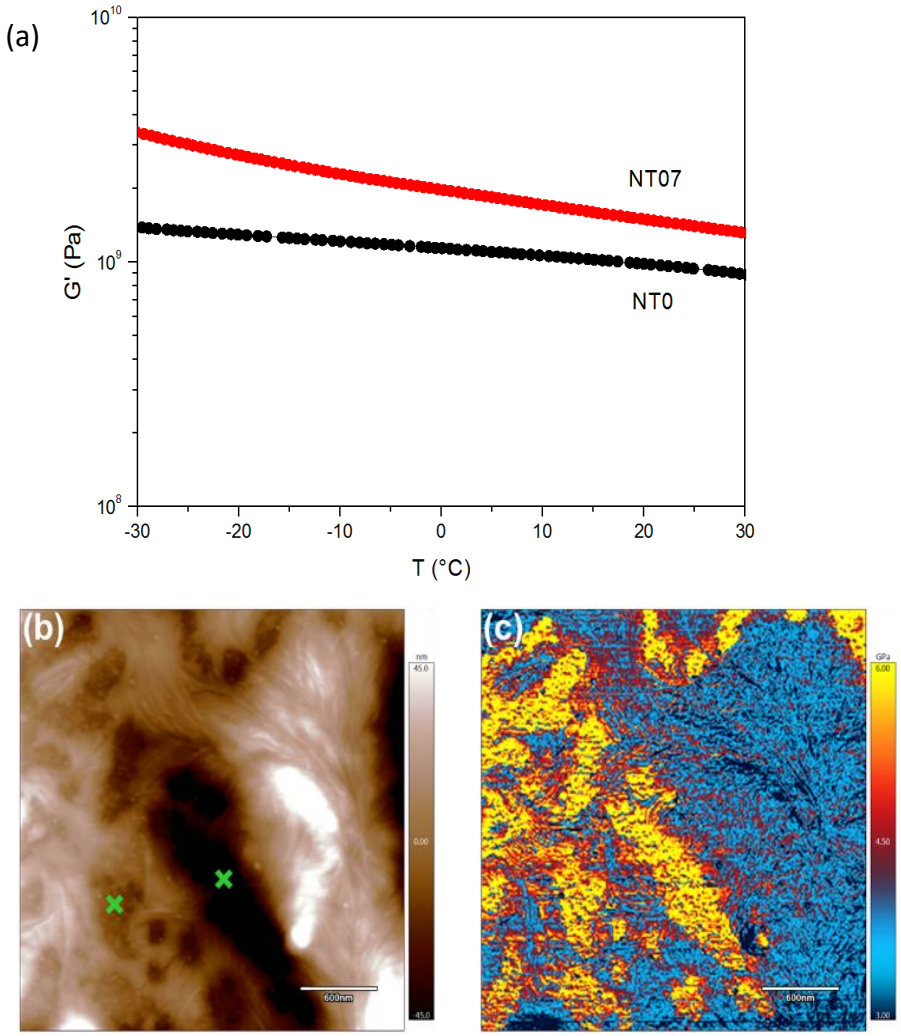

Figure 5. Mechanical behavior of the NT07 composite films. (a) Viscoelastic behavior recorded by DMA and compared to NT0. (b) AFM height and (c) corresponding AM-FM contact modulus images. The green crosses in (b) refer to the γ-phase regions.

At T = 20°C, G' has a value of 1 GPa for NT0 as compared to G' of the order of 1.5 GPa for NT07. In the latter case, the viscoelastic response primarily reflects the reinforcing effect of the CNTs even if the sample comprises both α- and γ-phases. Nanomechanical properties of NT07 thin film were then probed by mapping the AM-FM contact modulus over the surface of the sample. Figure 5b displays the surface morphology of NT07 sample where both α- and γ-phases have been observed (γ-phase regions identified by the green crosses). Corresponding modulus mapping is presented in Figure 5c. The contact modulus of the α-phase dominated area (blue

regions) is of the order of 3.1 GPa, whereas in the γ-phase (yellow regions) it amounts to 5.9 GPa. These elastic moduli were calculated by using the Hertzian model with punch tip geometry and radius of 8 nm. In this case, the average indentation value calculated during the nanomechanical experiments was found to be included between 0.5 and 0.9 nm for the γ and α phases respectively (see Figure S2b for the indentation map, and Figure S2c for the AM-FM contact modulus contrasts overlaid on the top of the 3D topography). This range of values is in agreement with the one obtained on the reference sample. From these results, since γ-PVDF is induced by the CNTs it is reasonable to consider that the nanoscale modulus reflects the local mechanical reinforcement by the CNTs. The reinforcing effect of the CNTs is thus confirmed at both macro- and nanoscales.

NT07 composite is of particular interest since it displays a maximum of PVDF γ-phase content. However looking for macroscopic piezoelectric properties, the composite is electrically conductive and the polar phase fraction is pretty low. Providing a specific nanoscale arrangement of nanotubes, for instance 2D CNT network, could allow the design of a distribution of high density electroactive "wires" in a non polar environment.

CONCLUSIONS

In summary, we report on the macro- and nanoscale investigations of PVDF-based nanocomposites for CNT loadings in the range 0 to 1.2 wt%. CNT incorporation mainly promotes the formation of the polar PVDF γ-phase and a maximum content is reached at 0.7% CNT content. AFM characterization of the latter sample clearly identifies at high resolution the spherulitic morphology of the PVDF α-phase with lamellar thickness around 10 nm. A peculiar morphology is also identified and attributed to the presence of the γ crystal phase by means of the PFM technique. The electromechanical behavior was probed in the PVDF γ-phase regions. It thus provides a robust answer to nanoscale phase identification and allows to assess the

piezoelectric activity in such a confined environment. The maximum effective piezoelectric coefficient was estimated to be $|d_{33}|$ ~13 pm/V, which paves the way for application of such PVDF-based composites as sensors, actuators or energy harvester systems. An increase in macroscopic conductivity with CNT content is observed, with a percolation threshold achieved for a composition close to NT07. It is postulated that beyond this composition, CNT aggregation reduces the capacity for γ-phase formation in relation to the decrease in interfacial area. The current detected locally reveals the presence of some infinite cluster homogeneously distributed over the NT07 surface. At the macroscopic level, the viscoelastic modulus is larger than that of neat PVDF, thus assessing the reinforcing effect of the CNTs. Nanoscale investigations reveal a higher contact modulus in the PVDF γ-phase regions, as compared to their α-phase counterparts. Considering that the γ-phase is induced by the presence of the CNTs, we may therefore conclude that the latter act both as a γ-phase nucleant and subsequently provide local mechanical reinforcement of the γ-phase regions. The direct identification of PVDF α- and γ-phases which was successfully achieved at the nanoscale, allowed a better understanding of impact of the CNTs on the structural and functional properties of the PVDF-based nanocomposites.

ASSOCIATED CONTENT

Supporting information

Additional data including contact-resonance curves during DART PFM experiments (Figure S1), AM-FM method and contact modulus (Figure S2), AFM image of thick NT07 (Figure S3) and isothermal crystallization of nanocomposites (Figure S4).

AUTHOR INFORMATION

Corresponding Author

*Sophie Barrau, E-mail : sophie.barrau@univ-lille1.fr

*Anthony Ferri, E-mail : anthony.ferri@univ-artois.fr

ACKNOWLEDGMENT

This work was partly supported through grant ANR-16-CE08-0025, ANR NanoPiC from French National Research Agency. The FE-SEM equipment has been implemented at the electron microscope facility (Institut Chevreul) thanks to the financial support of Région Hauts-de-France and European FEDER. The authors are grateful to Région Hauts-de-France and University of Lille for granting a PhD fellowship to J. Defebvin. Région Hauts-de-France and Fonds Européen de Développement Régional (FEDER) are also acknowledged for funding the MFP-3D microscope under Program “Chemistry and Materials for a Sustainable Growth”. The authors thank R. Barbattini from Asylum Research/Oxford Instruments for the AM-FM experiments.

REFERENCES

(1) Ueberschlag, P., PVDF piezoelectric polymer. *Sensor Review* **2001,** *21* (2), 118-126.

(2) Lovinger, A. J., Poly(Vinylidene Fluoride) In *Developments in Crystalline Polymers - 1*, Bassett, D. C., Ed. Springer, Dordrecht: 1982.

(3) Lovinger, A. J., Crystallization and morphology of melt-solidified poly(vinylidene fluoride) *Journal of polymer science. Part A-2, Polymer physics* **1980,** *18* (4), 793-809.

(4) Defebvin, J.; Barrau, S.; Stoclet, G.; Rochas, C.; Lefebvre, J.-M., In situ SAXS/WAXS investigation of the structural evolution of poly(vinylidene fluoride) upon uniaxial stretching. *Polymer* **2016,** *84*, 148-157.

(5) Lovinger, A. J., Unit cell of the gamma phase of poly(vinylidene fluoride). *Macromolecules* **1981,** *14* (2), 322-325.

(6) Li, W.; Meng, Q.; Zheng, Y.; Zhang, Z.; Xia, W.; Xu, Z., Electric energy storage properties of poly(vinylidene fluoride). *Applied Physics Letters* **2010,** *96* (19), 192905.

(7) Lovinger, A. J., Crystalline transformations in spherulites of poly(vinylidene fluoride). *Polymer* **1980,** *21* (11), 1317-1322.

(8) Prest Jr, W. M.; Luca, D. J., The formation of the gamma phase from the alpha and beta polymorphs of polyvinylidene fluoride. *Journal of Applied Physics* **1978,** *49* (10), 5042-5047.

(9) Ince-Gunduz, B. S.; Burke, K.; Koplitz, M.; Meleski, M.; Sagiv, A.; Cebe, P., Impact of Nanosilicates on Poly(vinylidene fluoride) Crystal Polymorphism: Part 2. Melt-crystallization at Low Supercooling. *Journal of Macromolecular Science, Part A* **2010,** *47* (12), 1208-1219.

(10) Lopes, A. C.; Costa, C. M.; Tavares, C. J.; Neves, I. C.; Lanceros-Mendez, S., Nucleation of the Electroactive gamma Phase and Enhancement of the Optical Transparency in Low Filler Content Poly(vinylidene)/Clay Nanocomposites. *The Journal of Physical Chemistry C* **2011,** *115* (37), 18076-18082.

(11) Lopes, A. C.; Caparros, C.; Gomez Ribelles, J. L.; Neves, I. C.; Lanceros-Mendez, S., Electrical and thermal behavior of gamma-phase poly(vinylidene fluoride)/NaY zeolite composites. *Microporous and Mesoporous Materials* **2012,** *161* (0), 98-105.

(12) Li, Y.; Xu, J.-Z.; Zhu, L.; Zhong, G.-J.; Li, Z.-M., Role of Ion-Dipole Interactions in Nucleation of Gamma Poly(vinylidene fluoride) in the Presence of Graphene Oxide during Melt Crystallization. *The Journal of Physical Chemistry B* **2012,** *116* (51), 14951-14960.

(13) Chae, D.; Hong, S., Rheology, crystallization behavior under shear, and resultant morphology of PVDF/multiwalled carbon nanotube composites. *Macromolecular Research* **2011,** *19* (4), 326-331.

(14) Sujoy Kumar, G.; Wahida, R.; Tapas Ranjan, M.; Shrabanee, S.; Dipankar, M., Improved breakdown strength and electrical energy storage performance of gamma-poly(vinylidene fluoride)/unmodified montmorillonite clay nano-dielectrics. *Nanotechnology* **2016,** *27* (21), 215401.

(15) Levi, N.; Czerw, R.; Xing, S.; Iyer, P.; Carroll, D. L., Properties of Polyvinylidene Difluoride-Carbon Nanotube Blends. *Nano Letters* **2004,** *4* (7), 1267-1271.

(16) Jia, N.; Xing, Q.; Xia, G.; Sun, J.; Song, R.; Huang, W., Enhanced beta-crystalline phase in poly(vinylidene fluoride) films by polydopamine-coated BaTiO3 nanoparticles. *Materials Letters* **2015,** *139*, 212-215.

(17) Serrado Nunes, J.; Wu, A.; Gomes, J.; Sencadas, V.; Vilarinho, P. M.; Lanceros-Mendez, S., Relationship between the microstructure and the microscopic piezoelectric response of the alpha- and beta-phases of poly(vinylidene fluoride). *Applied Physics A* **2009,** *95* (3), 875-880.

(18) Ting, Y.; Suprapto; Nugraha, A.; Chiu, C. W.; Gunawan, H., Design and characterization of one-layer PVDF thin film for a 3D force sensor. *Sensors and Actuators A: Physical* **2016,** *250*, 129-137.

(19) Zhiyuan, J.; Guangping, Z.; Ke, Z.; Zhuo, H.; Hao, W., Mechanisms of polarization switching in graphene oxides and poly(vinylidene fluoride)-graphene oxide films. *Japanese Journal of Applied Physics* **2016,** *55* (4S), 04EP04.

(20) Baji, A.; Mai, Y.-W.; Li, Q.; Liu, Y., Nanoscale investigation of ferroelectric properties in electrospun barium titanate/polyvinylidene fluoride composite fibers using piezoresponse force microscopy. *Composites Science and Technology* **2011,** *71* (11), 1435-1440.

(21) Liu, X.; Xu, S.; Kuang, X.; Tan, D.; Wang, X., Nanoscale investigations on beta-phase orientation, piezoelectric response, and polarization direction of electrospun PVDF nanofibers. *RSC Advances* **2016,** *6* (110), 109061-109066.

(22) Sharma, M.; Srinivas, V.; Madras, G.; Bose, S., Outstanding dielectric constant and piezoelectric coefficient in electrospun nanofiber mats of PVDF containing silver decorated multiwall carbon nanotubes: assessing through piezoresponse force microscopy. *RSC Advances* **2016,** *6* (8), 6251-6258.

(23) Rodriguez, B. J.; Callahan, C.; Kalinin, S. V.; Proksch, R., Dual-frequency resonance-tracking atomic force microscopy. *Nanotechnology* **2007,** *18* (47), 475504.

(24) Balke, N.; Bdikin, I.; Kalinin, S. V.; Kholkin, A. L., Electromechanical Imaging and Spectroscopy of Ferroelectric and Piezoelectric Materials: State of the Art and Prospects for the Future. *Journal of the American Ceramic Society* **2009,** *92* (8), 1629-1647.

(25) Garcia, R.; Proksch, R., Nanomechanical mapping of soft matter by bimodal force microscopy. *European Polymer Journal* **2013,** *49* (8), 1897-1906.

(26) Hurley, D.; Kocun, M.; Revenko, I.; Ohler, B.; Proksch, R., Fast, quantitative AFM nanomechanical measurements using AM-FM Viscoelastic Mapping Mode. *Microscopy and Analysis* **2015,** *29*, 9-13.

(27) Gannepalli, A.; Yablon, D. G.; Tsou, A. H.; Proksch, R., Mapping nanoscale elasticity and dissipation using dual frequency contact resonance AFM. *Nanotechnology* **2011,** *22* (35), 355705.

(28) Cai, X.; Lei, T.; Sun, D.; Lin, L., A critical analysis of the alpha, beta and gamma phases in poly(vinylidene fluoride) using FTIR. *RSC Advances* **2017,** *7* (25), 15382-15389.

(29) Gregorio, R., Determination of the α, β, and γ crystalline phases of poly(vinylidene fluoride) films prepared at different conditions. *Journal of Applied Polymer Science* **2006,** *100* (4), 3272-3279.

(30) Gregorio, R.; Ueno, E. M., Effect of crystalline phase, orientation and temperature on the dielectric properties of poly (vinylidene fluoride) (PVDF). *Journal of Materials Science* **1999,** *34* (18), 4489-4500.

(31) Davis, G. T.; McKinney, J. E.; Broadhurst, M. G.; Roth, S. C., Electric-field-induced phase changes in poly(vinylidene fluoride). *Journal of Applied Physics* **1978,** *49* (10), 4998-5002.

(32) Kumar, G. S.; Vishnupriya, D.; Chary, K. S.; Patro, T. U., High dielectric permittivity and improved mechanical and thermal properties of poly(vinylidene fluoride) composites with low carbon nanotube content: effect of composite processing on phase behavior and dielectric properties. *Nanotechnology* **2016,** *27* (38), 385702.

(33) Lotz, B.; Thierry, A.; Schneider, S., Origine moléculaire de l'enroulement des lamelles cristallines du poly(fluorure de vinylidène), phase gamma. *Comptes Rendus de l'Acadamie des Sciences - Series IIC - Chemistry* **1998,** *1* (10), 609-614.

(34) Vaughan, A. S., Etching and morphology of poly(vinylidene fluoride). *Journal of Materials Science* **1993,** *28* (7), 1805-1813.

(35) Martin, D.; Müller, J.; Schenk, T.; Arruda, T. M.; Kumar, A.; Strelcov, E.; Yurchuk, E.; Müller, S.; Pohl, D.; Schröder, U.; Kalinin, S. V.; Mikolajick, T., Ferroelectricity in Si-Doped

HfO2 Revealed: A Binary Lead-Free Ferroelectric. *Advanced Materials* **2014,** *26* (48), 8198-8202.

(36) McLachlan, M. A.; McComb, D. W.; Ryan, M. P.; Morozovska, A. N.; Eliseev, E. A.; Payzant, E. A.; Jesse, S.; Seal, K.; Baddorf, A. P.; Kalinin, S. V., Probing Local and Global Ferroelectric Phase Stability and Polarization Switching in Ordered Macroporous PZT. *Advanced Functional Materials* **2011,** *21* (5), 941-947.

(37) Liu, Y.; Weiss, D. N.; Li, J., Rapid Nanoimprinting and Excellent Piezoresponse of Polymeric Ferroelectric Nanostructures. *ACS Nano* **2010,** *4* (1), 83-90.

(38) Choi, Y.-Y.; Sharma, P.; Phatak, C.; Gosztola, D. J.; Liu, Y.; Lee, J.; Lee, B.; Li, J.; Gruverman, A.; Ducharme, S.; Hong, S., Enhancement of Local Piezoresponse in Polymer Ferroelectrics via Nanoscale Control of Microstructure. *ACS Nano* **2015,** *9* (2), 1809-1819.

(39) Kanik, M.; Aktas, O.; Sen, H. S.; Durgun, E.; Bayindir, M., Spontaneous High Piezoelectricity in Poly(vinylidene fluoride) Nanoribbons Produced by Iterative Thermal Size Reduction Technique. *ACS Nano* **2014,** *8* (9), 9311-9323.

(40) Ince-Gunduz, B. S.; Alpern, R.; Amare, D.; Crawford, J.; Dolan, B.; Jones, S.; Kobylarz, R.; Reveley, M.; Cebe, P., Impact of nanosilicates on poly(vinylidene fluoride) crystal polymorphism: Part 1. Melt-crystallization at high supercooling. *Polymer* **2010,** *51* (6), 1485-1493.

(41) Barrau, S.; Demont, P.; Maraval, C.; Bernes, A.; Lacabanne, C., Glass Transition Temperature Depression at the Percolation Threshold in Carbon Nanotube–Epoxy Resin and Polypyrrole–Epoxy Resin Composites. *Macromolecular Rapid Communications* **2005,** *26*, 390–394.

(42) Carponcin, D.; Dantras, E.; Dandurand, J.; Aridon, G. l.; Levallois, F.; Cadiergues, L.; Lacabanne, C., Discontinuity of physical properties of carbon nanotube/polymer composites at the percolation threshold. *Journal of Non-Crystalline Solids* **2014,** *392-393*, 19-25.

(43) Neidhöfer, M.; Beaume, F.; Ibos, L.; Bernès, A.; Lacabanne, C., Structural evolution of PVDF during storage or annealing. *Polymer* **2004,** *45* (5), 1679-1688.

SYNOPSIS

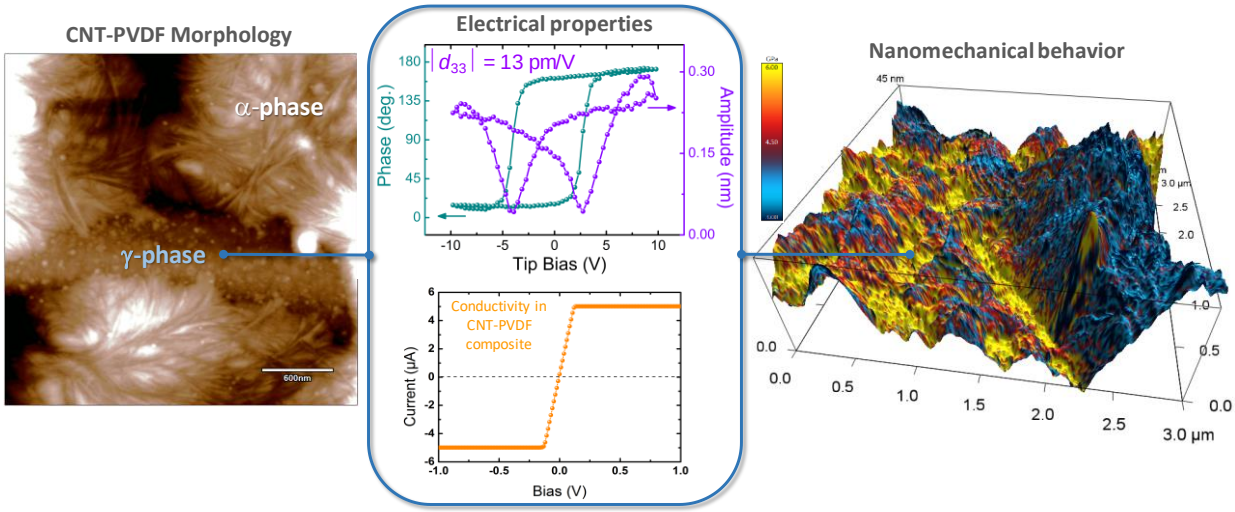
CNT-PVDF Morphology
α-phase
γ-phase
500nm
Electrical properties
|d33| = 13 pm/V
Phase (deg.)
Amplitude (nm)
Tip Bias (V)
Conductivity in CNT-PVDF composite
Current (μA)
Bias (V)
Nanomechanical behavior
45 nm
3.0 μm